Theory of end-labeled free-solution electrophoresis: Is the end effect important?

Mykyta V. Chubynsky and Gary W. Slater

Department of Physics, University of Ottawa,
150 Louis-Pasteur, Ottawa, Ontario, Canada, K1N 6N5

November 24, 2013

Corresponding author:
Dr. Mykyta V. Chubynsky
email: chubynsky@gmail.com
fax: +1-613-562-5190

Keywords:
ELFSE, elution time, end effect, FSCE, hydrodynamic interactions.

Abbreviations:

DT	Drag-tag
ELFSE	End-labeled free-solution electrophoresis
FSCE	Free-solution conjugate electrophoresis

Total number of words: 5720

Abstract

In the theory of free-solution electrophoresis of a polyelectrolyte (such as the DNA) conjugated with a "drag-tag", the conjugate is divided into segments of equal hydrodynamic friction and its electrophoretic mobility is calculated as a weighted average of the mobilities of individual segments. If all the weights are assumed equal, then for an electrically neutral drag-tag, the elution time t is predicted to depend linearly on the inverse DNA length $1/M$. While it is well-known that the equal-weights assumption is approximate and in reality the weights increase towards the ends, this "end effect" has been assumed to be small, since in experiments the $t(1/M)$ dependence seems to be nearly perfectly linear. We challenge this assumption pointing out that some experimental linear fits do not extrapolate to the free (i.e., untagged) DNA elution time in the limit $1/M \to 0$, indicating nonlinearity outside the fitting range. We show that a theory for a flexible polymer taking the end effect into account produces a nonlinear curve that, however, can be fitted with a straight line over a limited range of $1/M$ typical of experiments, but with a "wrong" intercept, which explains the experimental results without additional assumptions. We also study the influence of the flexibilities of the charged and neutral parts.

1 Introduction

Since the electrophoretic mobility of a uniformly charged polyelectrolyte (e.g., the DNA) is length-independent for all but the shortest lengths [1, 2], electrophoretic DNA separation is normally carried out in sieving media, such as gels or polymer solutions. A possible alternative, known as End-Labeled Free-Solution Electrophoresis (ELFSE) or Free-Solution Conjugate Electrophoresis (FSCE), is to attach the DNAs to identical objects (*drag-tags*) of a mobility different from that of the untagged DNA [3, 4, 5]. For instance, a neutral or a positively charged drag-tag would slow down the DNAs of different lengths by different amounts (the shorter the DNA, the more the influence of the drag-tag), thus leading to separation. Experimental tests of this idea have been conducted using different types of drag-tags, for example, a globular protein streptavidin [6, 7]; unfolded peptides, both neutral [8, 9, 10] and charged [11]; branched polypeptoids [12]; micelles serving as transiently bound drag-tags [13]; and gold nanoparticles [14]. To date, ELFSE has been used to separate ssDNA of up to 265 bases with single-base resolution [11], but further progress requires both experimental effort and better theoretical understanding. For the latter, theories and computer simulations of electrophoresis of composite objects are necessary. Besides generic theories not making specific assumptions about the drag-tag [3] and the simplest case of a flexible diblock copolymer [15, 16, 17, 18] in a weak field, the problems considered theoretically so far include globular [15, 19] and branched [20, 18] drag-tags, separation and stretching of a drag-tag–DNA composite in a strong field [21, 22, 23, 24], and drag-tags attached to both ends of the DNA [25]. Besides ELFSE, such studies can also be useful for understanding other situations of practical interest involving objects consisting of two or more parts with different electrophoretic properties, for instance, different variants of affinity electrophoresis [26, 27, 28, 29, 30].

Many of the theoretical treatments mentioned above are based on the theory of electrophoresis of polyampholytes developed by Long *et al.* [16, 31]. Suppose that the Debye length is sufficiently small and the polymer is sufficiently flexible that it can be divided into homogeneous pieces (or "blobs") each of which is a flexible coil, with the radii of gyration of all blobs being the same and much larger than the Debye length. The

polymer can then be represented as a Gaussian chain of beads with identical entropic springs connecting the beads, but, generally speaking, different electrophoretic mobilities of the beads (equal to the mobilities of the corresponding pieces). In that case, it was shown that the mobility of the polyampholyte is a *weighted average* of the mobilities of the individual beads [16, 31]:

$$\mu = \sum_{i=1}^{N} \Psi_i \mu_i, \tag{1}$$

where Ψ_i is the weight and μ_i the mobility of bead i, N is the total number of beads, and $\sum_{i=1}^{N} \Psi_i = 1$. If one further assumes that the weights of all the beads are equal,

$$\Psi_i = 1/N, \tag{2}$$

then for a diblock copolymer with N_1 beads in the first block and N_2 beads in the second block ($N_1 + N_2 = N$), the mobility is

$$\mu = \frac{N_1 \mu^{(1)} + N_2 \mu^{(2)}}{N_1 + N_2}, \tag{3}$$

where $\mu^{(1)}$ and $\mu^{(2)}$ are the mobilities of the blocks. In particular, if the first block is the DNA and the second one is a neutral drag-tag of a fixed length, then $\mu^{(1)} = \mu_{\mathrm{DNA}}$, $\mu^{(2)} = 0$, $N_1 \equiv N_{\mathrm{DNA}}$ is proportional to the DNA size in bases or base pairs, M, and $N_2 \equiv N_{\mathrm{DT}}$ is constant, so

$$\mu = \frac{M}{M + \alpha} \mu_{\mathrm{DNA}}, \tag{4}$$

where α is a constant characterizing the drag-tag. In a capillary electrophoresis experiment, the elution time t for a constant capillary length is inversely proportional to the mobility, and therefore,

$$t = \left(1 + \frac{\alpha}{M}\right) t_0, \tag{5}$$

where t_0 is the elution time of the untagged DNA. Thus, t is predicted to be linear in the inverse DNA length.

The equal-weights assumption is strictly true for a circular polymer, since in that case all beads are equivalent, but for a linear chain calculations show that the weights increase towards the chain ends and, in fact, diverge at the ends [31]. This is known as the *end effect* [16, 31, 32]. One would expect this to have some influence on the $t(1/M)$

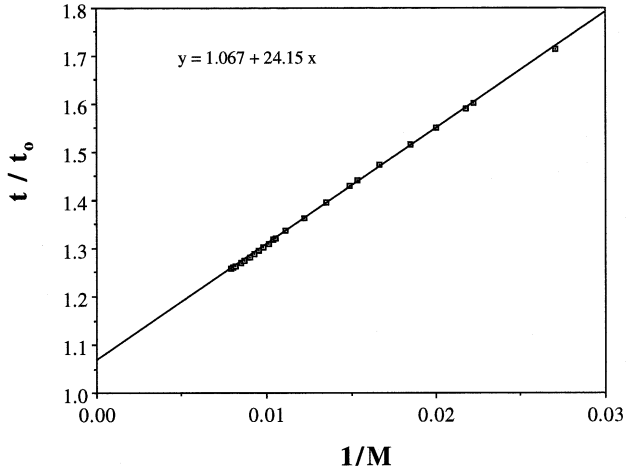

Figure 1: Experimental dependence of the ratio of the elution times of the ssDNA-drag-tag complex and the untagged ssDNA as a function of the inverse DNA size $1/M$. Streptavidin drag-tags were used. The line is a linear fit to the data (points). Reprinted from Ref. [7].

dependence. Surprisingly, published experimental data for ssDNA attached to a streptavidin drag-tag (reproduced in Fig. 1) give a nearly perfectly linear dependence, which seems to indicate (at least at first glance) perfect agreement with the simple theory neglecting the end effect. It is for this reason, perhaps, that the end effect was ignored in most theoretical considerations. One notable exception is a paper by McCormick and Slater [32], which, however, did not address explicitly the issue of the apparent linearity of the $t(1/M)$ dependence.

A closer inspection of Fig. 1 reveals, however, a striking peculiarity: contrary to what Eq. (5) predicts, the apparent intercept of the linear dependence of t/t_0 on $1/M$ is not unity. Obviously, as $1/M \to 0$, t/t_0 *should* approach unity, since the influence of the drag-tag should vanish in that limit. This is a common-sense result, independent of any particular theory. The only way to reconcile it with Fig. 1 (assuming that t_0 was measured correctly) is to admit the existence of some nonlinearity in the $t/t_0(1/M)$ dependence: the data for longer DNA (smaller $1/M$) should deviate from the straight line approaching $t/t_0 = 1$ as $1/M \to 0$. In Ref. [7], the deviation of the apparent intercept of the fit from unity was attributed to the residual EOF that may still exist despite the use of a coated

capillary. Another possibility is a charge on the drag-tag that would make the dependence nonlinear [3, 7]. While these possibilities cannot be ruled out completely, we argue in this article that the result in Fig. 1 can be explained entirely by the end effect, without assuming the existence of an EOF or a drag-tag charge. Our explanation seems all the more likely given that a very similar result (linearity with a "wrong" intercept) was also observed in a different experiment with a different drag-tag (a branched polypeptoid) [12].

The structure of this paper is as follows. In the next section we review the approach we use for calculating the end effect, which is essentially identical to that used by Long *et al.* [16, 31]. In Sec. 3 we first present our results for the mobility of a flexible diblock copolymer and then compare to the cases when the polymer is semiflexible, a rigid rod, and also when either part is rigid and the other is flexible. We end the paper with a discussion and the outlook.

2 A Zimm model for the end effect

We first review the approach of Long *et al.* [16, 31], adapting the Zimm model of polymer dynamics [33].

Consider a set of connected beads placed in a stagnant fluid of viscosity η in a uniform electric field $\mathbf{E}$. The connections can be entropic springs, but they can also be rigid rods and, in fact, the whole set can form a rigid rod or an object of another shape — this is unimportant for our general considerations. What is important is that the set of beads moves as a single object on average. There are four types of forces acting on each bead. First, the electrophoretic force, which would move a single bead i taken alone with the velocity $\mu_i\mathbf{E}$, where μ_i is the electrophoretic mobility of the bead. Second, the mechanical force $\mathbf{F}_i$ due to the connections of bead i with other beads. Third, there is a drag force $-\zeta_i(\mathbf{V}_i - \mathbf{V}_i^0)$, where ζ_i is the mechanical friction coefficient of bead i, $\mathbf{V}_i$ is the velocity of the bead, and $\mathbf{V}_i^0$ is the velocity of the fluid in the vicinity of bead i due to the motion of other beads. Fourth, there is a random (thermal) force $\boldsymbol{\xi}_i$ that vanishes on average. In the

overdamped limit, the total force on the bead should be zero, and this gives

$$\mathbf{V}_i = \mu_i \mathbf{E} + (\mathbf{F}_i + \boldsymbol{\xi}_i)/\zeta_i + \mathbf{V}_i^0. \tag{6}$$

The fluid velocity $\mathbf{V}_i^0$ is given approximately by

$$\mathbf{V}_i^0 \approx \sum_{j \neq i} \hat{H}_{ij}(\mathbf{F}_j + \boldsymbol{\xi}_j), \tag{7}$$

where

$$\hat{H}_{ij} = \frac{1}{8\pi\eta r_{ij}} \left(\hat{I} + \frac{\mathbf{r}_{ij} \otimes \mathbf{r}_{ij}}{r_{ij}^2} \right), \quad i \neq j, \tag{8}$$

is the Oseen tensor [34]. Here $\hat{I}$ is the unit tensor and $\mathbf{r}_{ij}$ is the vector connecting beads i and j. Defining also the diagonal elements $\hat{H}_{ii}$ as $1/\zeta_i$, we can rewrite Eq. (6) as

$$\mathbf{V}_i = \mu_i \mathbf{E} + \sum_j \hat{H}_{ij}(\mathbf{F}_j + \boldsymbol{\xi}_j). \tag{9}$$

Averaging both sides of this equation, we get

$$\langle \mathbf{V}_i \rangle = \mu_i \mathbf{E} + \sum_j \langle \hat{H}_{ij}(\mathbf{F}_j + \boldsymbol{\xi}_j) \rangle. \tag{10}$$

We now make a crucial assumption, known as the *Kirkwood-Riseman approximation* [34], that $\langle \hat{H}_{ij}(\mathbf{F}_j + \boldsymbol{\xi}_j) \rangle \approx \langle \hat{H}_{ij} \rangle \langle (\mathbf{F}_j + \boldsymbol{\xi}_j) \rangle = \langle \hat{H}_{ij} \rangle \langle \mathbf{F}_j \rangle$, and thus,

$$\mathbf{V} = \langle \mathbf{V}_i \rangle \approx \mu_i \mathbf{E} + \sum_j \langle \hat{H}_{ij} \rangle \langle \mathbf{F}_j \rangle. \tag{11}$$

Here we have used the fact that all beads move together on average, and thus their average velocities are identical, $\langle \mathbf{V}_i \rangle \equiv \mathbf{V}$. If all directions of $\mathbf{r}_{ij}$ are equiprobable, the Oseen tensor becomes a scalar after averaging:

$$\langle \hat{H}_{ij} \rangle \equiv H_{ij} = \frac{\delta_{ij}}{\zeta_i} + \frac{1}{6\pi\eta} \left\langle \frac{1}{r_{ij}} \right\rangle (1 - \delta_{ij}), \tag{12}$$

where δ_{ij} is the Kronecker delta symbol. Solving Eq. (11) for $\langle \mathbf{F}_i \rangle$, we get

$$\langle \mathbf{F}_i \rangle \approx \sum_j G_{ij}(\mathbf{V} - \mu_j \mathbf{E}), \tag{13}$$

where the matrix G is the inverse of the matrix H:

$$G_{ij} = (H^{-1})_{ij}. \tag{14}$$

Summing over all beads,

$$\mathbf{F} \approx \sum_{i,j} G_{ij}(\mathbf{V} - \mu_j \mathbf{E}), \tag{15}$$

where $\mathbf{F}$ is the sum of all mechanical forces acting on the beads, which is equal to the external mechanical force on the system. If there is no such external force ($\mathbf{F} = 0$) and our set of beads only moves due to the electric field, then

$$\mathbf{V} = \frac{\sum_{i,j} G_{ij}\mu_j}{\sum_{i,j} G_{ij}}\mathbf{E} \tag{16}$$

and for the mobility $\mu = V/E$ we get Eq. (1) with the weights

$$\Psi_j = \frac{\sum_i G_{ij}}{\sum_{i,j} G_{ij}}. \tag{17}$$

Conversely, when there is no electric field ($\mathbf{E} = 0$), but $\mathbf{F} \neq 0$, we get

$$\mathbf{F} = \sum_{i,j} G_{ij}\mathbf{V}, \tag{18}$$

and thus

$$\zeta = \sum_{i,j} G_{ij} \tag{19}$$

is the mechanical friction coefficient, as first calculated for a Gaussian chain by Zimm [33].

According to Eq. (17), all that is required to calculate the weights Ψ_j is to find the averaged Oseen tensor matrix H_{ij} and invert it numerically to get G_{ij}. For the numerical inversion we have used the LAPACK software library [35]. Calculating H_{ij} using Eq. (12) requires knowing the average inverse distances $\langle 1/r_{ij} \rangle$. In some cases, these are known analytically. For example, for a Gaussian chain (i.e., a chain without excluded volume interactions) with beads numbered sequentially along the chain,

$$\left\langle \frac{1}{r_{ij}} \right\rangle = \frac{1}{b}\sqrt{\frac{6}{\pi|i-j|}}, \tag{20}$$

where b is the root-mean-square distance between adjacent beads [34]. For a rigid rod, all distances are deterministic and if b is the distance between adjacent beads, then

$$\left\langle \frac{1}{r_{ij}} \right\rangle = \frac{1}{b|i-j|}. \tag{21}$$

In other cases, for instance, for a semiflexible polymer, $1/\langle r_{ij}\rangle$ can be calculated numerically, by sampling different conformations of the polymer. The diagonal elements, H_{ii}, require the friction coefficients of the beads, ζ_i. However, at least for a Gaussian chain in the long-chain limit we expect the polymer friction coefficient $\zeta = \sum_{i,j} G_{ij}$ to be simply proportional to the radius of gyration of the polymer and independent of the properties of the individual beads. Thus, in this limit, presumably, the weights proportional to $\sum_i G_{ij}$ are also independent of ζ_i, which we have confirmed numerically. Therefore, ζ_i are essentially free parameters (although, if they are chosen too large, the matrix H can become singular [36]). It is convenient to choose ζ_i so that ζ converges to its infinite-chain value calculated by Zimm [33] as rapidly as possible as the chain size is increased. As an arbitrary but convenient choice, we assume that the beads are spherical, so their frictions are $\zeta_i = 6\pi\eta a$, where a is the radius of the spheres (identical for all beads). We find then that the optimal choice is $a \approx 0.25b$. For a rigid rod, it is natural to identify a with the radius of the rod. Then the theoretical friction of the rod averaged over all directions is [37]

$$\zeta = \frac{3\pi\eta N b}{\ln(Nb/a)}. \tag{22}$$

Note that unlike for a chain, ζ for a rod should depend on a (albeit only logarithmically). Unfortunately, that dependence is not reproduced in this simple approach. When we put $b = 1$, $\eta = 1$, fix a and fit the $\zeta(N)$ dependence we obtain with

$$\zeta = \frac{A_0 N}{\ln(N/A_1)}, \tag{23}$$

where A_0 and A_1 are fitting constants, then, while for A_0 we do get values close to 3π, as expected, we find that A_1, instead of changing linearly with a, actually has a much stronger (exponential) dependence, with $A_1 \approx 0.62$ for $a = 0.5$, $A_1 \approx 0.01$ for $a = 0.1$, and $A_1 \sim 10^{-22}$ for $a = 0.01$. On the other hand, we do find that for $a = 0.25$ $A_1/a \approx 1$. Thus, fixing a at $0.25b$ is again an appropriate choice, and we use this value for all our calculations.

3 Results for the end effect

3.1 A flexible chain

For a flexible Gaussian chain, Long *et al.* [31] found numerically using the method described in the previous section that the weights Ψ_i increase towards the ends of the chain and diverge at the ends. Ultimately, this is due to the fact that beads at the ends have fewer other beads nearby and therefore their hydrodynamic interaction with the rest of the chain is weaker [31, 32].

In the long-chain limit ($N \gg 1$), the weights become N-independent in the sense that it is possible to introduce a continuous and N-independent function $\psi(x)$ with $0 < x < 1$ and $\int_0^1 \psi(x)dx = 1$, such that

$$\Psi_i = \psi\left(\frac{i-1/2}{N}\right)\Big/N. \tag{24}$$

In the same continuum limit, the mobility of the polymer can be found as

$$\mu = \int_0^1 \psi(x)\mu(x)dx, \tag{25}$$

where $\mu(x)$ is the intrinsic mobility of the part of the polymer whose distance from the end along the contour is a fraction x of the total contour length. Long *et al.* [31] found numerically that for $x \to 0$ $\psi(x)$ diverges as $x^{-1/4}$ (and similarly for $x \to 1$), but did not provide a full analytical expression for $\psi(x)$ valid for all x. McCormick and Slater [32] used an approximate expression for this purpose. In fact, it turns out that there is a remarkably simple *exact* expression for $\psi(x)$:

$$\psi(x) = Cx^{-1/4}(1-x)^{-1/4}, \tag{26}$$

where $C = \sqrt{\pi}/[2\Gamma^2(3/4)]$ is a normalization constant and Γ is the gamma function. This function $\psi(x)$ is plotted in Fig. 2 together with the numerical results obtained by inverting the average hydrodynamic interaction matrix for Gaussian chains with $N = 20$ and 50, as explained in the previous section. The agreement is excellent and gets better as N gets larger. Moreover, although it is not immediately apparent, this result can be found in

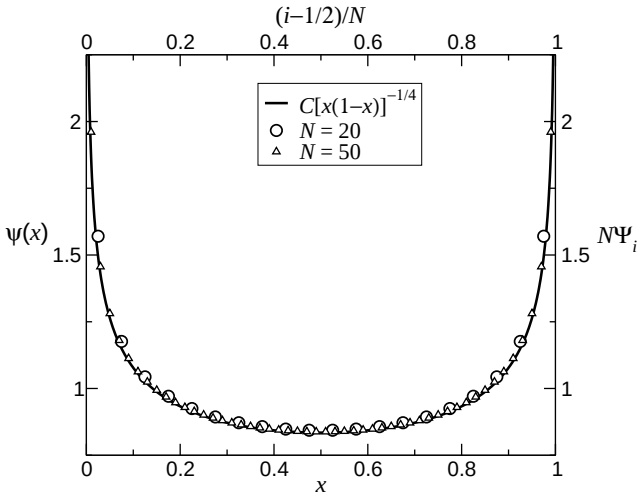

Figure 2: Scaled weights $N\Psi_i$ (top x-axis and right y-axis) obtained numerically for Gaussian chains of two different sizes. The line is $\psi(x)$ (left y-axis and bottom x-axis) given by Eq. (26).

Zimm's original 1956 paper [33] [see Eq. (92b) in that paper, which, up to a normalization factor, is the inverse of our $\psi(x)$, given that Zimm's polymer contour variable r runs from -1 to 1 and thus $r = 2x - 1$].

For the DNA of length M attached to a neutral drag-tag of a fixed length,

$$\mu(x) = \begin{cases} \mu_{\rm DNA}\,, & 0 < x < M/(M+\alpha), \\ 0\,, & M/(M+\alpha) < x < 1, \end{cases} \tag{27}$$

where $\alpha = \text{const}$. If the end effect is neglected, $\psi(x) \equiv 1$, and Eq. (25) gives Eq. (4), as expected. On the other hand, using Eq. (26), we get

$$\mu = \mu_{\rm DNA} \int_0^{M/(M+\alpha)} Cx^{-1/4}(1-x)^{-1/4}dx = \mu_{\rm DNA} \frac{\int_0^{M/(M+\alpha)} x^{-1/4}(1-x)^{-1/4}dx}{\int_0^1 x^{-1/4}(1-x)^{-1/4}dx}, \tag{28}$$

or for the elution time,

$$t = t_0 \frac{\int_0^1 x^{-1/4}(1-x)^{-1/4}dx}{\int_0^{1/(1+\alpha/M)} x^{-1/4}(1-x)^{-1/4}dx}. \tag{29}$$

Note that t/t_0 is a function of α/M only. Equation (29) can be expressed through the hypergeometric function [38], but it is also easy to simply calculate the integrals numerically for different values of α/M. Still, it is instructive to consider analytically the

limits of a small ($M \ll \alpha$) and large ($M \gg \alpha$) DNA. In the first case, only small x enter the integral in the denominator of Eq. (29). Then $x^{-1/4}(1-x)^{-1/4} \approx x^{-1/4}$, which gives

$$\frac{t}{t_0} \approx \frac{\int_0^1 x^{-1/4}(1-x)^{-1/4}dx}{\int_0^{M/\alpha} x^{-1/4}dx} = \frac{3\Gamma^2(3/4)}{2\sqrt{\pi}}(\alpha/M)^{3/4} \approx 1.27(\alpha/M)^{3/4},\ M \ll \alpha. \tag{30}$$

In the second case,

$$\begin{aligned} \frac{t}{t_0} &\approx \frac{\int_0^1 x^{-1/4}(1-x)^{-1/4}dx}{\int_0^1 x^{-1/4}(1-x)^{-1/4}dx - \int_{1-\alpha/M}^1 (1-x)^{-1/4}dx} \\ &\approx 1 + \frac{2\sqrt{\pi}}{3\Gamma^2(3/4)}(\alpha/M)^{3/4} \approx 1 + 0.79(\alpha/M)^{3/4},\ M \gg \alpha. \end{aligned} \tag{31}$$

Thus for large M, $(t/t_0 - 1) \propto (\alpha/M)^{3/4}$ and likewise for small M, $(t/t_0 - 1) \approx t/t_0 \propto (\alpha/M)^{3/4}$, although the proportionality factors are different. The large-M result is particularly interesting, since it shows explicitly that not only is there a nonlinearity in contrast to Eq. (5), but even the exponent in the limit $M \to \infty$ is different from unity. The derivative dt/dM is proportional to $M^{-7/4}$ instead of M^{-2} expected for the linear dependence. Since this derivative determines the peak resolution of the device, it is expected to be better for large M than the theory ignoring the end effect predicts. This has already been pointed out by Slater and McCormick [32]; a new result is that, at least in theory, the resolution should be *infinitely* better at large M, since $M^{-7/4}/M^{-2} \to \infty$ for $M \to \infty$, although how useful this is in practice is not obvious.

In Fig. 3 the solid curve shows t/t_0 calculated numerically using Eq. (29) as a function of α/M. It is seen that the dependence is strongly nonlinear, in contrast to that given by Eq. (5) (which neglects the end effect) shown as a dotted line. Most strikingly, the slope of the solid line becomes infinite in the limit $\alpha/M \to 0$, as expected for the $(\alpha/M)^{3/4}$ dependence. However, to compare to Fig. 1 we also included a linear fit (shown as a dashed line) to the solid line in a limited range (indicated by the short vertical lines) chosen so that t/t_0 varies between ≈ 1.25 and ≈ 1.75, just as in Fig. 1 We note that the linear fit is quite good in this range, but if the straight line is extrapolated to zero, the intercept differs significantly from unity. Both these features are qualitatively similar to Fig. 1. In fact, the slight curvature in the fitting range is also consistent with the data in Fig. 1 (this curvature was mentioned in Ref. [7]). Quantitatively, the intercept is slightly higher (1.079 vs. 1.067),

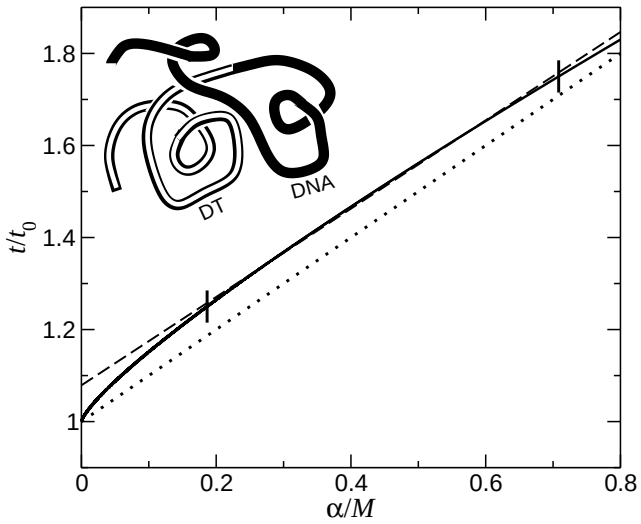

Figure 3: Theoretical dependence of the ratio of the elution times of the DNA–drag-tag complex and the untagged DNA as a function of the normalized inverse DNA size. The dotted line is Eq. (5), which corresponds to neglecting the end effect. The solid line takes the end effect into account assuming that both parts are flexible [Eq. (29)]. The dashed line is a linear fit to the solid line in the interval indicated by the two short vertical lines. The DNA–drag-tag complex is drawn schematically at the top, with the drag-tag (DT) and DNA parts indicated.

but this discrepancy is not surprising, given that we have assumed that the drag-tag is a flexible polymer, whereas in Ref. [7] a globular protein was used. In fact, the ssDNA cannot be considered completely flexible either, as its persistence length, while small compared to, say, dsDNA, is still significantly larger than its thickness. Our result does show that the explanation of results in Fig. 1 based on the end effect is plausible.

However, it is still desirable to study the sensitivity of the result to the properties of the polymer and, in particular, to its stiffness. This is done in the next section. An additional motivation for this study is provided by the results of Heller *et al.* [6] for the *double-stranded* DNA, which is much stiffer than ssDNA. In this case the intercept of the linear fit was found to be much closer to unity (in fact, even slightly below unity; see Fig. 1 in Ref. [6]). To compare different cases, we use the intercept of the linear fit to the $t/t_0(1/M)$ dependence with the fitting interval chosen as described above as a convenient

measure of the strength of the end effect: the closer the intercept to unity, the weaker the end effect. For brevity, we will always be referring to the neutral part as the drag-tag and the charged part as the DNA, even though we will be dealing with model systems whose properties are very different from those of the actual drag-tags used so far and the DNA.

3.2 A rigid rod and a semiflexible chain

We now consider the opposite case of a stiff rod polymer. We assume that the whole DNA–drag-tag complex is a single rigid rod with a charged part representing the DNA and the neutral part representing the drag-tag. We first calculate the weights Ψ_i numerically, as described in Sec. 2. The result for three different sizes N is shown in Fig. 4(a). First of all, we find that unlike the case of a flexible chain, where for sufficiently large N the rescaled weights fall onto a universal, N-independent curve [see Eq. (24) and Fig. 2], here the part of the rod where the end effect is significant becomes progressively smaller (relative to the total rod length) as N increases. Essentially, the end effect vanishes in the long-rod limit (assuming that the thickness of the rod stays constant). This is actually related to the known fact from the hydrodynamic slender-body theory [39] that the density of the force exerted by the fluid on a moving rod is constant along the rod [note that Eq. (13) with $\mathbf{E} = 0$ can be rewritten as $\langle \mathbf{F}_i \rangle \propto \Psi_i \mathbf{V}$]. Moreover, even for a finite N the divergence of the weights at the ends is not as strong as for a flexible chain (logarithmic instead of power-law). The data in Fig. 4(a) can be fitted with

$$\Psi_i = \sqrt{\frac{\ln BN/4}{\ln B(i-1/2)[1-(i-1/2)/N]}}, \tag{32}$$

where $B = 13.34$. This form shows that the absolute length of the regions near the ends where the weights are significantly higher is N-independent (thus the *relative* length goes as $1/N$).

Figure 4(b) shows the result of the calculation of t/t_0 as a function of the ratio of the drag-tag length N_{DT} and the DNA length N_{DNA}, for the drag-tag length $N_{\mathrm{DT}} = 50$ beads. Unsurprisingly, the nonlinearity is much weaker, and the intercept of the linear fit (not

shown in the figure) is much closer to unity (1.028 instead of 1.079), which may explain the dsDNA result in Ref. [6].

For comparison, Fig. 4(b) also shows the same dependence for a *semiflexible* chain, with both parts having persistence length $p = 5$ segments. For the bead radius $a = 0.25$ and the segment length $b = 1$, this corresponds to the persistence length of about $pb/2a = 10$ chain thicknesses, which is similar to (perhaps a bit higher than) that of a ssDNA [19]. To calculate $\langle 1/r_{ij} \rangle$ in this case, for each data point we generate 1000 or 10000 conformations of a freely rotating chain [40] using the standard expression for the angle θ between adjacent bonds,

$$\cos\theta = \exp(-1/p). \tag{33}$$

The nonlinearity is stronger than for a rod, but much weaker than for a flexible chain (with the curve for the latter repeated in this figure as a dotted line for ease of comparison). This result shows that even a small amount of stiffness (similar to that of a ssDNA) can lead to a large reduction of the end effect, even when the drag-tag length (which is $N_{\rm DT} = 50$ in our calculation) is ten times larger than the persistence length of both the drag-tag and the DNA. While at first glance this casts a doubt on the explanation of the results in Fig. 1 in terms of the end effect, one has to keep in mind that unlike in our model, in the experiment the ssDNA and the drag-tag had very different stiffnesses, with the drag-tag being an essentially completely rigid globule. To make a more valid comparison, in the next section we study the case when the DNA and the drag-tag have different stiffnesses (although, unlike the experimental situation, the drag-tag is still linear).

3.3 A rod-coil conjugate

Consider now the case of a stiff rod attached to a flexible Gaussian chain (a coil). Assume that the first N_1 beads belong to the rod and the rest N_2 belong to the coil. To calculate $\langle 1/r_{ij} \rangle$, obviously, when both beads i and j belong to the coil part, Eq. (20) can be used, and when both belong to the rod part, Eq. (21) can be used. When bead i belongs to the

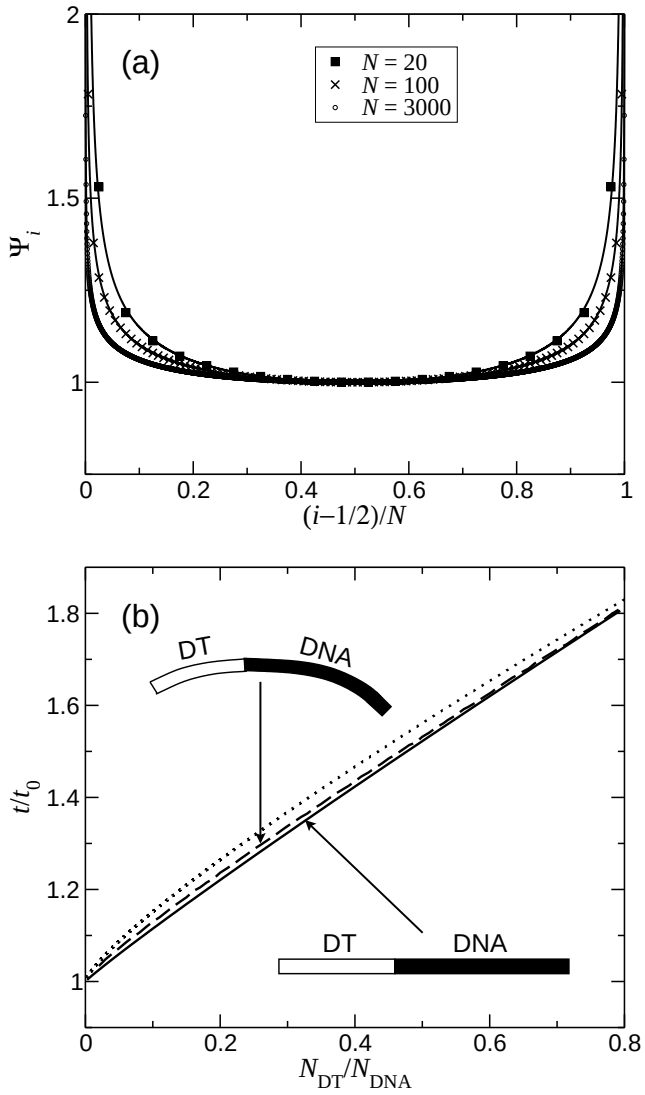

Figure 4: (a) Scaled weights Ψ_i obtained numerically for rigid rods of three different sizes, normalized for ease of comparison so that the value in the middle of the rod is always unity. The lines are given by Eq. (32). (b) Dependence of the ratio of the elution times of the DNA–drag-tag complex and the untagged DNA as a function of the ratio of the drag-tag and DNA sizes. The solid line is for a stiff rod [drawn schematically at the bottom, with the drag-tag (DT) and the DNA parts marked]; the dashed line is for a semiflexible chain (drawn at the top) with persistence length $p = 5$ and the drag-tag length $N_{\rm DT} = 50$ (see the text for details); the dotted line is for a flexible chain. The first two lines are calculated using the weights obtained numerically, except for the lowest $1/N_{\rm DNA}$ values for the stiff rod, where Eq. (32) was used. The third line was obtained using Eq. (29). Note that the stiffness of the semiflexible chain is strongly exaggerated in the drawing.

rod and bead j belongs to the coil, $\langle 1/r_{ij} \rangle$ can still be calculated analytically:

$$\left\langle \frac{1}{r_{ij}} \right\rangle = \frac{\int_{r=0}^{\infty} \int_{\theta=0}^{\pi} \frac{r^2 \exp[-3r^2/2(j-N_1)] \sin\theta}{\sqrt{(N_1-i)^2+r^2-2(N_1-i)r\cos\theta}} dr d\theta}{\int_0^{\infty} 2r^2 \exp[-3r^2/2(j-N_1)] dr} = \frac{\mathrm{erf}\left((N_1-i)\sqrt{\frac{3}{2(j-N_1)}}\right)}{N_1-i}, \tag{34}$$

where for simplicity the segment lengths $b_1 = b_2 = 1$ and erf is the error function.

Figure 5 shows the t/t_0 dependence on the inverse DNA length $1/N_{\mathrm{DNA}}$, both for the case when the DNA is flexible and the drag-tag is rigid (which models the situation in Ref. [7] and Fig. 1) and for the opposite case when the DNA is rigid and the drag-tag is flexible (which represents better the case of unfolded peptide drag-tags [8, 9, 10] that are more flexible than even ssDNA). In the first case, the nonlinearity is extremely high, with the intercept of the linear fit at 1.123, even higher than for a flexible chain, while the fit itself is rather poor. Conversely, in the second case the dependence is very close to linear for small and moderate $1/N_{\mathrm{DNA}}$, with the intercept essentially equal to unity.

The striking difference between the two cases seems all the more peculiar when one realizes that they are not unrelated, but are, in a way, "mirror images" of one another. For a rod-coil conjugate with N_1 beads in the rod part and N_2 beads in the coil part, the mobility is given by

$$\mu = \Gamma(N_1/N_2)\mu_1 + [1 - \Gamma(N_1/N_2)]\mu_2, \tag{35}$$

where μ_1 and μ_2 are the mobilities of the respective parts and the weight $\Gamma(N_1/N_2)$ of the rod part is a function of N_1/N_2 only. When the rod part is charged ("the DNA") and the coil part is neutral ("the drag-tag"), this expression reduces to

$$\mu_{\underline{\mathrm{rod}}+\mathrm{coil}} = \Gamma(N_{\mathrm{DNA}}/N_{\mathrm{DT}})\mu_{\mathrm{DNA}}. \tag{36}$$

Here and below the charged part is underlined in the subscript. Similarly, when the rod part is the drag-tag and the coil part is the DNA, we obtain

$$\mu_{\underline{\mathrm{coil}}+\mathrm{rod}} = [1 - \Gamma(N_{\mathrm{DT}}/N_{\mathrm{DNA}})]\mu_{\mathrm{DNA}}. \tag{37}$$

The corresponding elution times are

$$\frac{t_{\underline{\mathrm{rod}}+\mathrm{coil}}}{t_0} = \frac{1}{\Gamma(N_{\mathrm{DNA}}/N_{\mathrm{DT}})} \tag{38}$$

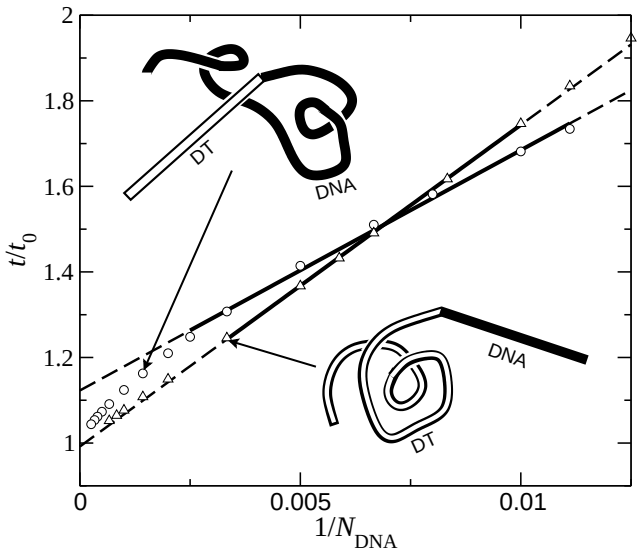

Figure 5: Dependence of the ratio of the elution times of the DNA–drag-tag complex and the untagged DNA as a function of the inverse DNA size, for the case when the drag-tag part is stiff with a fixed length $N_{\mathrm{DT}}^{\mathrm{rod}} = 20$ and the DNA is a flexible coil (circles; see the corresponding schematic drawing at the top with the parts labeled) and for the case when the drag-tag is flexible with $N_{\mathrm{DT}}^{\mathrm{coil}} = 500$ and the DNA is stiff (triangles; drawing at the bottom). Note that the hydrodynamic radii of the drag-tags ($\sim N_{\mathrm{DT}}^{\mathrm{rod}}$ and $\sim \sqrt{N_{\mathrm{DT}}^{\mathrm{coil}}}$, respectively) are similar in these cases. All data points are calculated numerically, as described in Sec. 2, using average inverse distances given by Eqs. (20), (21), and (34). The dashed lines are the linear fits, with the actual ranges used for fitting shown as thicker solid lines.

and

$$\frac{t_{\underline{\text{coil}}+\text{rod}}}{t_0} = \frac{1}{1-\Gamma(N_{\text{DT}}/N_{\text{DNA}})}. \tag{39}$$

Therefore, the behavior of $t_{\underline{\text{rod}}+\text{coil}}/t_0$ at small $1/N_{\text{DNA}}$ is related to that of $t_{\underline{\text{coil}}+\text{rod}}/t_0$ at large $1/N_{\text{DNA}}$ and vice versa. In particular, it is easy to check that if $t_{\underline{\text{rod}}+\text{coil}}/t_0$ were linear for *all* $N_{\text{DT}}/N_{\text{DNA}}$ with slope c, then $t_{\underline{\text{coil}}+\text{rod}}/t_0$ would have been linear as well, with slope $1/c$. Therefore, the nonlinearity of the latter apparent in Fig. 5 is the consequence of the nonlinearity of the former at large $1/N_{\text{DNA}}$, outside the range of the plot and thus not obvious from it.

4 Summary and discussion

We have studied the influence of the hydrodynamic end effect on the mobility of a block copolymer consisting of a neutral ("the drag-tag") and a charged ("the DNA") blocks, in particular, its dependence on the DNA length M. The theory neglecting the end effect predicts a linear dependence of the elution time t on $1/M$; the nonlinearity of this dependence is a measure of significance of the end effect. Looking at the effect of stiffness of different parts, we find that this nonlinearity is strongest when the drag-tag is stiff and the DNA is flexible, weaker when both parts are flexible, still weaker when both are rigid, and the weakest when the drag-tag is flexible and the DNA is rigid. We also find that in the case when both parts are flexible, even a slight increase in stiffness leads to a significant decrease of the nonlinearity. At the same time, we have also noted that even in the cases when the nonlinearity is rather strong (except perhaps in the case when it is the strongest), linear fits over relatively narrow ranges of $1/M$ typical of experiments can be quite successful. On the other hand, in the limit of very large M, the dependence is particularly strongly nonlinear, with even the exponent being different [$(t/t_0) - 1 \propto M^{-3/4}$], except when the DNA is completely stiff, in which case the exponent appears to be unity in this limit.

We believe that these findings are important for interpreting the results of a variety of ELFSE experiments, especially since the stiffness of both the drag-tag (rigid globular

proteins vs. flexible unfolded peptides) and the DNA (more stiff dsDNA vs. more flexible ssDNA) varies between different experiments. In particular, for the experiment with ssDNA and a globular protein drag-tag [7] (reproduced in Fig. 1 in this paper), both the linear dependence of $t/t_0(1/M)$ in the experimental range of M and the fact that the intercept is significantly higher than unity can be explained by the end effect. Of all situations we have studied, the closest to this experiment is the one with a rigid drag-tag and a completely flexible DNA. While in that particular case the nonlinearity is too strong for a good linear fit and the intercept of the (poor) fit is much higher than in the experiment, we recall that both the nonlinearity and the intercept should decrease when the stiffness of the DNA is taken into account and that even the ssDNA stiffness is sufficient to change the intercept significantly. The result for the completely flexible case, for which the intercept is lower and close to that observed experimentally, shows that in that case the linear fit is quite successful. Our results also explain why the intercept is lower for a stiffer dsDNA, as observed in Ref. [6].

Of course, it should be remembered that a globular drag-tag in Refs. [6, 7] is not the same as a rigid rod, and therefore extending the consideration to the case when the drag-tag is a solid (e.g., spherical) object is desirable. This is also relevant for micellar drag-tags [13]. While it is not immediately obvious that the approach of this paper is applicable to solid objects, our preliminary results show that it is and the results for large M are qualitatively and in some respects even quantitatively similar to those for a rod. Still, there appear to be a lot of interesting details that we will discuss in a future publication. Another case of interest is that of a branched drag-tag, as in Ref. [12].

For the situation when the DNA and the drag-tag have different mechanical properties, we have only considered the extreme case when one of the parts is completely flexible and the other completely rigid. In previous works neglecting the end effect [...], the case of semiflexible parts with different persistence lengths was treated by dividing both parts into "blobs" of equal hydrodynamic radii, treating each blob as the new "effective monomer" and thus reducing the problem to that of a flexible chain with a constant monomer size. This reduction should still apply in principle even when the end effect is taken into account, *but* only if it is possible to subdivide both parts into blobs in such a way that *both*

the number of persistence lengths per blob is large and the number of blobs is large as well. This means that it is only strictly applicable when the length of each part is much, *much* (and we cannot emphasize *much* enough!) larger than its persistence length. We note in this respect that in our consideration of a semiflexible chain, the length of the drag-tag (50) was quite large compared to the persistence length (5), yet the result was still significantly different from that for the fully flexible chain.

A related approach used in the past [19] for situations involving a single neutral rigid object attached to a flexible DNA coil divides the coil into blobs of the same hydrodynamic radius (or, equivalently, the same hydrodynamic friction) as that of the rigid object and then treats the whole conjugate as a flexible chain with the object treated as one of the blobs, on equal footing with other blobs. Implicitly, this corresponds to assuming that when the hydrodynamic frictions of the neutral object and the DNA are the same, the mobility of the conjugate is equal to one half of the DNA mobility. Using our approach, we can check if this is the case for a rod-coil conjugate, since it allows us to calculate both the mobility and the frictions of the parts. We find that for the rod length of 20 monomers, the DNA length at which the mobility is 1/2 of the DNA mobility is about 58, while the length at which the frictions are equal is only slightly different at 63, so this assumption is indeed rather accurate. Of course, as mentioned, for the resulting chain of blobs to be fully equivalent to a long flexible chain (including the end effect), the number of resulting blobs needs to be large (a situation unlikely to be encountered in practice).

In our considerations for flexible and semiflexible chains, we have considered them as phantom chains neglecting excluded volume. Taking this into account is likely to modify the exponent making it slightly higher than 3/4, but should not change the results qualitatively otherwise.

One should also keep in mind that the approach we use is itself approximate, in particular, because it involves the Kirkwood-Riseman approximation. Recently, Hickey *et al.* [41, 42] have found that the predictions of the theory of Long *et al.* [31] agree qualitatively with their simulations; in particular, they have verified the overall shape of the weight function in Fig. 2 [42]. There are still some quantitative discrepancies, but they may come at least

in part from approximations and assumptions of the simulation method itself. More research in this direction is needed.

Experimental verification of our results should be relatively straightforward. Of particular interest in this respect would be extending ELFSE experiments to much larger DNA sizes (even if single-base resolution cannot be achieved for them) to study the elution time dependence at very small $1/M$. Another issue is the dependence of the end effect on the stiffness of the DNA and the drag-tag, which can be studied by using different kinds of drag-tags, as well as both ssDNA and dsDNA, and perhaps even replacing the DNA with another polyelectrolyte (either more flexible or more stiff).

5 Acknowledgments

We thank Dr. Owen A. Hickey (Stuttgart) and the members of our group for useful discussions. We acknowledge financial support from the University of Ottawa and the Natural Sciences and Engineering Research Council of Canada (NSERC).

6 Conflict of interest statement

The authors declare no conflicts on interest.

References

[1] Viovy, J.-L., *Rev. Mod. Phys.* 2000, *72*, 813–872.

[2] Shendruk, T. N., Hickey, O. A., Slater, G. W., Harden, J. L., *Curr. Opin. Colloid Interface Sci.* 2012, *17*, 74–82.

[3] Mayer, P., Slater, G. W., Drouin, G., *Anal. Chem.* 1994, *66*, 1777–1780.

[4] Meagher, R. J., Won, J.-I., McCormick, L. C., Nedelcu, S., Bertrand, M. M., Bertram, J. L., Drouin, G., Barron, A. E., Slater, G. W., *Electrophoresis* 2005, *26*, 331–350.

[5] Coyne, J. A., Lin, J. S., Barron, A. E., in: Landers, J. P. (Ed.), *Handbook of Capillary and Microchip Electrophoresis and Associated Microtechniques*, 3rd ed., CRC Press, Boca Raton, FL, U.S.A. 2008, pp. 381–412.

[6] Heller, C., Slater, G. W., Mayer, P., Dovichi, N., Pinto, D., Viovy, J.-L., Drouin, G., *J. Chromatogr. A* 1998, *806*, 113–121.

[7] Ren, H., Karger, A. E., Oaks, F., Menchen, S., Slater, G. W., Drouin, G., *Electrophoresis* 1999, *20*, 2501–2509.

[8] Won, J.-I., Meagher, R. J., Barron, A. E., *Biomacromolecules* 2004, *5*, 618–627.

[9] Won, J.-I., Meagher, R. J., Barron, A. E., *Electrophoresis* 2005, *26*, 2138–2148.

[10] Meagher, R. J., Won, J.-I., Coyne, J. A., Lin, J., Barron, A. E., *Anal. Chem.* 2008, *80*, 2842–2848.

[11] Albrecht, J. C., Lin, J. S., Barron, A. E., *Anal. Chem.* 2011, *83*, 509–515.

[12] Haynes, R. D., Meagher, R. J., Won, J.-I., Bogdan, F. M., Barron, A. E., *Bioconjugate Chem.* 2005, *16*, 929–938.

[13] Savard, J. M., Grosser, S. T., Schneider, J. W., *Electrophoresis* 2008, *29*, 2779–2789.

[14] Cao, W., Chen, L., Fu, Y., Tan, Z., Qu, B., *J. Sep. Sci.* 2011, *34*, 939–946.

[15] Long, D., Ajdari, A., *Electrophoresis* 1996, *17*, 1161–1166.

[16] Long, D., Viovy, J.-L., Ajdari, A., *J. Phys.: Condens. Matter* 1996, *8*, 9471–9475.

[17] McCormick, L. C., Slater, G. W., Karger, A. E., Vreeland, W. N., Barron, A. E., Desruisseaux, C., Drouin, G., *J. Chromatogr. A* 2001, *924*, 43–52.

[18] Grass, K., Holm, C., Slater, G. W., *Macromolecules* 2009, *42*, 5352–5359.

[19] Desruisseaux, C., Long, D., Drouin, G., Slater, G. W., *Macromolecules* 2001, *34*, 44–52.

[20] Nedelcu, S., Slater, G. W., *Electrophoresis* 2005, *26*, 4003–4015.

[21] McCormick, L. C., Slater, G. W., *Electrophoresis* 2007, *28*, 674–682.

[22] McCormick, L. C., Slater, G. W., *Electrophoresis* 2007, *28*, 3837–3844.

[23] Nedelcu, S., Meagher, R. J., Barron, A. E., Slater, G. W., *J. Chem. Phys.* 2007, *126*, 175104.

[24] Lau, H. W., Archer, L. A., *Phys. Rev. E* 2010, *81*, 031918.

[25] Meagher, R. J., McCormick, L. C., Haynes, R. D., Won, J.-I., Lin, J. S., Slater, G. W., Barron, A. E., *Electrophoresis* 2006, *27*, 1702–1712.

[26] Schou, C., Heegaard, N. H. H., *Electrophoresis* 2006, *27*, 44–59.

[27] Berezovski, M. V., Krylov, S. N., in: Landers, J. P. (Ed.), *Handbook of Capillary and Microchip Electrophoresis and Associated Microtechniques*, 3rd ed., CRC Press, Boca Raton, FL, U.S.A. 2008, pp. 361–380.

[28] Zhu, Z., Ravelet, C., Perrier, S., Guieu, V., Roy, B., Perigaud, C., Peyrin, E., *Anal. Chem.* 2010, *82*, 4613–4620.

[29] Wegman, D. W., Krylov, S. N., *Angew. Chem. Int. Ed.* 2011, *50*, 10335–10339.

[30] Tsukada, H., Watanabe, T., Kanayama, N., Takarada, T., Maeda, M., *Electrophoresis* 2012, *33*, 2122–2129.

[31] Long, D., Dobrynin, A. V., Rubinstein, M., Ajdari, A., *J. Chem. Phys.* 1998, *108*, 1234–1244.

[32] McCormick, L. C., Slater, G. W., *Electrophoresis* 2005, *26*, 1659–1667.

[33] Zimm, B. H., *J. Chem. Phys.* 1956, *24*, 269–278.

[34] Kirkwood, J. G., Riseman, J., *J. Chem. Phys.* 1948, *16*, 565–573.

[35] Anderson, E., Bai, Z., Bischof, C., Blackford, S., Demmel, J., Dongarra, J., Du Croz, J., Greenbaum, A., Hammarling, S., McKenney, A., Sorensen, D., *LAPACK Users' Guide*, 3rd ed., Society for Industrial and Applied Mathematics, Philadelphia, PA, U.S.A. 1999.

[36] Zwanzig, R., Kiefer, J., Weiss, G. H., *Proc. Natl. Acad. Sci. U.S.A.* 1968, *60*, 381–386.

[37] Berg, H. C., *Random Walks in Biology*, 2nd ed., Princeton University Press, Princeton, NJ, U.S.A. 1998.

[38] The integral in the denominator of Eq. (29) is reduced to a particular case of Eq. (15.6.1) in F. W. J. Olver, D. W. Lozier, R. F. Boisvert, C. W. Clark (Eds.), *NIST Handbook of Mathematical Functions*, Cambridge University Press, New York 2010, by a trivial substitution.

[39] Batchelor, G. K., *J. Fluid Mech.* 1970, *44*, 419–440.

[40] Rubinstein, M., Colby, R. H., *Polymer Physics*, Oxford University Press, Oxford; New York 2003.

[41] Hickey, O. A., Holm, C., Harden, J. L., Slater, G. W., *Phys. Rev. Lett.* 2010, *105*, 148301.

[42] Hickey, O. A., Holm, C., *J. Chem. Phys.* 2013, *138*, 194905.

Figure captions

Figure 1

Experimental dependence of the ratio of the elution times of the ssDNA-drag-tag complex and the untagged ssDNA as a function of the inverse DNA size $1/M$. Streptavidin drag-tags were used. The line is a linear fit to the data (points). Reprinted from Ref. [7].

Figure 2

Scaled weights $N\Psi_i$ (top x-axis and right y-axis) obtained numerically for Gaussian chains of two different sizes. The line is $\psi(x)$ (left y-axis and bottom x-axis) given by Eq. (26).

Figure 3

Theoretical dependence of the ratio of the elution times of the DNA–drag-tag complex and the untagged DNA as a function of the normalized inverse DNA size. The dotted line is Eq. (5), which corresponds to neglecting the end effect. The solid line takes the end effect into account assuming that both parts are flexible [Eq. (29)]. The dashed line is a linear fit to the solid line in the interval indicated by the two short vertical lines. The DNA–drag-tag complex is drawn schematically at the top, with the drag-tag (DT) and DNA parts indicated.

Figure 4

(a) Scaled weights Ψ_i obtained numerically for rigid rods of three different sizes, normalized for ease of comparison so that the value in the middle of the rod is always unity. The lines

are given by Eq. (32). (b) Dependence of the ratio of the elution times of the DNA–drag-tag complex and the untagged DNA as a function of the ratio of the drag-tag and DNA sizes. The solid line is for a stiff rod [drawn schematically at the bottom, with the drag-tag (DT) and the DNA parts marked]; the dashed line is for a semiflexible chain (drawn at the top) with persistence length $p = 5$ and the drag-tag length $N_{\rm DT} = 50$ (see the text for details); the dotted line is for a flexible chain. The first two lines are calculated using the weights obtained numerically, except for the lowest $1/N_{\rm DNA}$ values for the stiff rod, where Eq. (32) was used. The third line was obtained using Eq. (29). Note that the stiffness of the semiflexible chain is strongly exaggerated in the drawing.

Figure 5

Dependence of the ratio of the elution times of the DNA–drag-tag complex and the untagged DNA as a function of the inverse DNA size, for the case when the drag-tag part is stiff with a fixed length $N_{\rm DT}^{\rm rod} = 20$ and the DNA is a flexible coil (circles; see the corresponding schematic drawing at the top with the parts labeled) and for the case when the drag-tag is flexible with $N_{\rm DT}^{\rm coil} = 500$ and the DNA is stiff (triangles; drawing at the bottom). Note that the hydrodynamic radii of the drag-tags ($\sim N_{\rm DT}^{\rm rod}$ and $\sim \sqrt{N_{\rm DT}^{\rm coil}}$, respectively) are similar in these cases. All data points are calculated numerically, as described in Sec. 2, using average inverse distances given by Eqs. (20), (21), and (34). The dashed lines are the linear fits, with the actual ranges used for fitting shown as thicker solid lines.